

Low-dimensional chaos in the single wave model for self-consistent wave-particle Hamiltonian

J. V. Gomes,^{1,2, a)} M. C. de Sousa,^{3,2, b)} R. L. Viana,^{1, c)} I. L. Caldas,^{3, d)} and Y. Elskens^{2, e)}

¹⁾Universidade Federal do Paraná, Departamento de Física, 81531-980, Curitiba, Paraná - Brazil

²⁾Aix-Marseille Université, CNRS, PIIM UMR 7345, 13397 Marseille - France

³⁾Universidade de São Paulo, Instituto de Física, 05508-090, São Paulo, São Paulo - Brazil

We analyze nonlinear aspects of the self-consistent wave-particle interaction using Hamiltonian dynamics in the single wave model, where the wave is modified due to the particle dynamics. This interaction plays an important role in the emergence of plasma instabilities and turbulence. The simplest case, where one particle ($N = 1$) is coupled with one wave ($M = 1$), is completely integrable so that all trajectories are regular and the nonlinear effects reduce to the wave potential pulsating while the particle remains either trapped or circulating forever. On increasing the number of particles ($N = 2, M = 1$), integrability is lost, and chaos appears and becomes more intense close to the hyperbolic fixed point, in the homoclinic tangle born from the separatrix, whereas it could gradually reduce near elliptic fixed points. However, we also observe the emergence of atypical chaos near the elliptic fixed points.

Wave-particle interaction plays an important role in plasma dynamics both in the laboratory and in space. The processes resulting from the interaction between charged particles and waves are related to the emergence of instability and turbulence in plasmas. In the phase space, this interaction can generate both regular trajectories, which may lead to coherent particle acceleration, and chaotic trajectories, which are responsible for particle heating and escape. Low-dimensional approximations often shed light on the dynamics of systems with many degrees of freedom, as chaotic motion arises as one increases the number of degrees of freedom. In the simplest case, one particle ($N = 1$) is coupled to one wave ($M = 1$) in a self-consistent way, such that the wave is also modified due to the particle dynamics. This case is completely integrable, so that all trajectories are regular and the nonlinear effects degenerate to particle trapping while the wave potential pulsates. The bifurcation diagram of this simple system displays a saddle-center coalescence and a special role of the trajectory for which the wave intensity goes through zero. On increasing the number of particles ($N = 2, M = 1$), chaos arises due to the strong sensitivity in the initial condition of the relative velocity of the particles. As this case is a non-integrable Hamiltonian system, chaos is already expected to start and become more intense in the regions close to the hyperbolic fixed point, since its homoclinic tangle is always chaotic. Following this idea, chaos should gradually reduce as the trajectories approach the elliptic fixed point. However, chaotic trajectories can also appear near the elliptic fixed point for a negative energy regime.

I. INTRODUCTION

Wave-particle interaction is one of the characteristic phenomena that occur naturally in plasma physics and play an essential role in their dynamics.^{1,2} Plasmas are naturally conducive to the amplification and propagation of waves due to their intrinsic characteristic of trying to restore balance in the local distribution of charges when the system is exposed to disturbances.³ Attempts to make plasmas return to equilibrium can intensify a diversity of wave modes, with characteristic frequencies, which are able to propagate in the plasma and interact with particles whose velocities are close to the phase velocity.⁴ Hamiltonian systems provide a rich description of this interaction, where the regular and chaotic behavior of the particles trajectories in their phase space are directly related to the amplitude of the disturbance applied to the system.^{5,6}

The exchange of energy and momentum through wave-particle interaction is especially important in rarefied plasmas where the collision time between charged particles is generally very long compared to the characteristic time scales of the system, and therefore those plasmas can be treated as non-collisional.⁷ At first, this implies that, in practice, there is no energy dissipation in low-density plasmas, since collisions are rare. However, the presence of waves can induce finite dissipation even in non-collisional plasmas:^{8,9} plasma particles are scattered by the wave fields, and their energies and momenta change through such processes.

In general terms, effective finite dissipation in collisionless plasmas occurs via resonance and can give rise, for example, to the growth/damping of waves and heating/acceleration of particles, as well as to the transport of charged particles.^{2,10,11} The interaction becomes stronger when the streaming velocity of the particles is such that the particle couples with the Doppler-shifted wave at its cyclotron frequency or its harmonics. This is the so-called cyclotron resonance interaction.¹² The special case of the Doppler-shifted wave frequency being zero (*i.e.* zero harmonic of the cyclotron frequency) corresponds to the well-known Landau resonance.¹³

In practice, Landau damping (*resp.* growth) can be understood as follows: as observed experimentally,¹⁴ particles with

^{a)}Electronic mail: janygovi@gmail.com

^{b)}Electronic mail: meirielenso@gmail.com

^{c)}Electronic mail: viana@fisica.ufpr.br

^{d)}Electronic mail: ibere@if.usp.br

^{e)}Electronic mail: yves.elskens@univ-amu.fr

velocities slightly lower (greater) than the phase velocity of a wave are accelerated (decelerated) by the wave's electric field. Thus, the particles that move a little slower (faster) than the phase velocity gain (lose) energy from (to) the wave.¹⁵

The main concepts described by Landau are widely used in particle accelerators to avoid instabilities in the coherent oscillation of the beams.¹⁶ Besides, aspects of this interaction are notoriously important in space plasma physics, such as in the suprathermal electron acceleration at the solar wind,¹⁷ in the interaction of charged particles with the Earth's magnetic field,¹⁸ etc. For this reason, even many decades after its discovery,¹⁹ there is high interest in the fundamental aspects related to Landau damping.^{20,21}

An important feature of this type of interaction is that ions, being much more massive than electrons, are assumed to be fixed and their role is limited to providing charge neutrality for the system. The collective vibration of electrons with respect to ions is called Langmuir waves.⁴ The usual description of the interaction of Langmuir waves with electrons whose velocities are close to their phase velocity involves the kinetic set of Vlasov-Poisson equations for the electron distribution function.²²

In order to describe the interaction between charged particles and electrostatic waves, it is natural to use Hamiltonian models for which the particle dynamics in phase space generates both regular and chaotic trajectories.^{5,6} The predominance of either type of trajectory depends mainly on the amplitude of the perturbation in the system that directly influences the motion of the particles.^{23,24} In general, regions where regular trajectories prevail are more favorable to coherent particle acceleration, while chaotic regions are associated with particle heating and escape.²⁵

Wave-particle interactions have often been described by Hamiltonian models in which particle motion is affected by the wave field, whereas the wave itself is not influenced by particle motion.^{5,6} However, proper treatment of the problem would require also the addition of the wave response to the particle motion, which leads to so-called self-consistent Hamiltonians.^{1,26} In this framework, the dynamics of Langmuir waves is described as M harmonic oscillators coupled to N quasi-resonant particles. Considering the single wave model (SWM) introduced by Onishchenko, O'Neil, and coworkers,^{27,28} it is possible to study the chaotic dynamics of wave-particle self-consistent interaction in terms of a few degrees of freedom. Indeed, this model can even be reduced to a four degrees of freedom system to describe its saturation regime,^{29,30} and the model with a single particle was already considered by Adam, Laval and Mendonça³¹ with a view at its integrability and at the generation of sideband modes of the Langmuir waves.

The SWM originates from the description of the beam-plasma instability, and since then this model has proven to be relevant in a variety of physical situations in which the dynamics is effectively dominated by a single mode as in the confinement of charged particles in tokamaks,³² Landau damping,³³ free-electron lasers,^{30,34} in the relationship between self-consistent chaos and phase space coherent structures,³⁵ and in the kinetic instabilities of the Alfvén wave-particle interac-

tion obtained experimentally in tokamak JET.³⁶

In the present work, we revisit the dynamics of the single wave model with one particle ($N = 1$), which is integrable, so that the phase portrait comprises only regular trajectories. The bifurcation diagram, in this case, shows a saddle-center coalescence that occurs for a specific value of the total momentum P and divides the phase portrait topologies. Moreover, we stress the role of the trajectory for which the wave intensity I passes through zero, and we find a specific value of the total momentum for which this trajectory coincides with a branch of the separatrix.

For two particles ($N = 2$), we study the emergence of low-dimensional chaos. We observe that the intensification of chaotic activity occurs both in the domains close to the hyperbolic fixed point (as expected) and in the region close to the elliptic fixed point (an atypical fact). Fourier analysis shows that the non-linear evolution of the particles motion, close to the elliptic fixed point, gives rise to the appearance and intensification of resonances. We find that the contribution of the resonances eventually becomes sufficient for the appearance of chaos, even for small fluctuations in the potential. Near the hyperbolic point, the system is highly chaotic, as expected, since in this non-integrable system, the separatrix found for $N = 1$ has generated a homoclinic tangle. The chaotic activity in this region is called separatrix chaos.³⁷

Our numerical computations were performed using a leap-frog symplectic integrator, which conserves the geometry of the system exactly and its energy quite accurately for long time.³⁸ For the non-integrable case with two particles, we studied the dynamics by intercepting the trajectories with a Poincaré section.³⁹

This article is organized as follows: in the next section (II), we present the single wave Hamiltonian. The dynamics for one particle ($N = 1$) is analyzed in section III. The chaotic dynamics for $N = 2$ is discussed in section IV. The last section (V) is devoted to our conclusions and prospects.

II. THE SINGLE WAVE HAMILTONIAN

The self-consistent dynamics of N identical particles moving on the interval of length L with periodic boundary conditions, interacting with M longitudinal waves with wave numbers $k_j = j2\pi/L$ and natural frequencies ω_{0j} , is described by the reference Hamiltonian^{1,9}

$$H_{sc}^{N,M} = \sum_{r=1}^N \frac{p_r^2}{2m_r} + \sum_{j=1}^M \omega_{0j} \frac{X_j^2 + Y_j^2}{2} + \epsilon \sum_{r=1}^N \sum_{j=1}^M k_j^{-1} \beta_j (Y_j \sin k_j x_r - X_j \cos k_j x_r), \quad (1)$$

$$H_{sc}^{N,M} = \sum_{r=1}^N \frac{p_r^2}{2m_r} + \sum_{j=1}^M \omega_{0j} I_j + \epsilon \sum_{r=1}^N \sum_{j=1}^M k_j^{-1} \beta_j \sqrt{2I_j} \cos(k_j x_r - \theta_j), \quad (2)$$

where β_j is the coupling constant of wave j and ε is the overall coupling parameter. Here, $Z_j = X_j + iY_j = \sqrt{2I_j}e^{-i\theta_j}$, the generalized coordinates are the particles positions x_r and waves phases θ_j , and their conjugate momenta are the particles momenta p_r and waves intensities I_j . In phasor formulation, the generalized waves coordinates are the X_j with conjugate momenta Y_j .

The Hamiltonian $H_{sc}^{N,M}$ comprises three contributions: the free motion (kinetic energy) of the particles, the (harmonic) oscillation of the waves, and the coupling between particles and waves. Besides that, the Hamiltonian $H_{sc}^{N,M}$ is invariant under translation in time and in space so that the total energy $E = H_{sc}^{N,M}$ and the total momentum $P = \sum_{r=1}^N p_r + \sum_{j=1}^M k_j I_j$ are conserved. The latter constant reveals that the growth or decay of a wave is directly balanced with the slowing down or acceleration of particles.

We focus on a single special case, where all particles have the same mass, and we rescale time and energy to set the coupling constant $\varepsilon\beta_1$ and the particles mass m equal to unity in Eq. (3). In the single wave model ($M = 1$), we omit the subscript j and set the length unit to k^{-1} and the spatial period to $L = 2\pi$, which reduces the Hamiltonian to

$$H_{sc}^N = \sum_{r=1}^N \frac{p_r^2}{2} + \omega_0 I - \sqrt{2I} \sum_{r=1}^N \cos(x_r - \theta). \quad (3)$$

A Galileo transformation enables us to put the system in the reference frame of the wave. With the generating function $F_1(x, \theta, \bar{p}, \bar{I}, t) = \sum_{r=1}^N (x_r - \omega_0 t)(\bar{p}_r + \omega_0) + (\theta - \omega_0 t)\bar{I} - N\omega_0^2 t/2$, the Hamiltonian (3) becomes

$$\begin{aligned} \bar{H}(\bar{p}, \bar{I}, \bar{x}, \bar{\theta}) &= H_{sc}^N + \frac{\partial F_1}{\partial t} \\ &= \sum_{r=1}^N \frac{\bar{p}_r^2}{2} - \sqrt{2\bar{I}} \sum_{r=1}^N \cos(\bar{x}_r - \bar{\theta}). \end{aligned} \quad (4)$$

Total momentum

$$\bar{P} = \sum_{r=1}^N \bar{p}_r + \bar{I} \quad (5)$$

is conserved by the dynamics obtained from Eq. (4). This enables us to define a new generating function $F_2(\bar{x}, \bar{\theta}, p', I') = I'\bar{\theta} + \sum_{r=1}^N p'_r(\bar{x}_r - \bar{\theta})$: the new coordinate conjugate to $p'_r = \bar{p}_r$ is $x'_r = \partial F_2 / \partial p'_r = (\bar{x}_r - \bar{\theta})$, which we denote as $y_r = x'_r$, and the new momentum conjugate to $\theta' = \bar{\theta}$ is $I' = \bar{P}$. The latter is a constant of motion so that the new angle $\theta' = \bar{\theta}$ is a cyclic coordinate. The final Hamiltonian, emphasizing that only N degrees of freedom are effective, is obtained in the compact form

$$H(p, y) = \sum_{r=1}^N \frac{p_r^2}{2} - \sqrt{2I} \sum_{r=1}^N \cos y_r, \quad (6)$$

where, for short, we dropped the prime from p'_r and the overbars from $\bar{I} = \bar{P} - \sum_r p'_r$ and from \bar{H} .

The wave-particle interaction is typical in many physical systems, and we investigate in this paper how this particular form of coupling given by the Hamiltonian (6) affects the

dynamics of the particles as we increase the number of degrees of freedom. This single wave Hamiltonian was first formulated as a simplified model to treat the instability due to a weak cold electron beam in a plasma, assuming a fixed ionic neutralizing background.^{27,28} More recently, different studies extended the application of the single wave model to a much larger class of instabilities,⁴⁰ derived it in a generic manner from different contexts, and proved it could model various phenomena in fluids and plasmas,³⁵ and Compton free-electron laser amplification.⁴¹

III. THE SINGLE WAVE WITH ONE PARTICLE

In order to understand this system, we start with a few degrees of freedom. We first study the simplest, integrable case^{29,31,42} for this model where the self-consistency couples one particle and one wave, $M = N = 1$. As we will see in section IV, the dynamics for $N = 2$ incorporates most of the basic phenomena that we will discuss in the next two subsections. Moreover, the dynamics with $N = 1$ bears fundamental importance in the description of phenomena for the case with many particles,^{29,31} where the macroparticle is used to describe the dynamics of an electron beam so that the beam electrons oscillate bunched in the bottom of the wave potential well during the trapping process.²⁷⁻³⁰

A. Preliminary analysis of the dynamics for $N = M = 1$

The single wave Hamiltonian for this case reads

$$H = \frac{p^2}{2} + (Y \sin x - X \cos x) = \frac{p^2}{2} - \sqrt{2I} \cos(x - \theta), \quad (7)$$

and the conserved total momentum is $P = p + I$. The evolution equations

$$\dot{x} = p, \quad (8a)$$

$$\dot{p} = -X \sin x - Y \cos x = -\sqrt{2I} \sin(x - \theta), \quad (8b)$$

$$\dot{X} = \sin x, \quad (8c)$$

$$\dot{Y} = \cos x, \quad (8d)$$

imply that $\dot{X}^2 + \dot{Y}^2 = 1$ so that the wave never remains still. Besides, $\ddot{p} = -1 + (Y \sin x - X \cos x)p$.

For this simple case with only one particle, the single wave Hamiltonian has two degrees of freedom, one for the particle and one for the wave. As the Hamiltonian is invariant under space translations, the momentum conservation law reduces the problem to one degree of freedom. To express this, we introduce $y = x - \theta$ and write the Hamiltonian in the form

$$H = \frac{p^2}{2} - \sqrt{2(P-p)} \cos y, \quad (9)$$

with I expressed in terms of the particle momentum. As this Hamiltonian is time-independent, the system is completely integrable. In particular, the particle orbits in the phase portrait follow the constant energy contours ($H = \text{constant}$).

The equations of motion of the Hamiltonian (9) read

$$\dot{y} = p + \frac{1}{\sqrt{2(P-p)}} \cos y, \quad (10a)$$

$$\dot{p} = -\sqrt{2(P-p)} \sin y. \quad (10b)$$

The fixed points of the system are defined by the conditions

$$\dot{y} = \partial_p H = 0, \quad \dot{p} = -\partial_y H = 0. \quad (11)$$

Solving these conditions for the Hamiltonian (9), we obtain the coordinates (y_i^*, p_i^*) of the fixed points C_i^*

$$C_1^* : (0, p_1^* \sqrt{2(P-p_1^*)} = -1), \quad (12a)$$

$$C_{2,3}^* : (\pi, p_{2,3}^* \sqrt{2(P-p_{2,3}^*)} = 1), \quad (12b)$$

with $p_1^* < 0$, $0 < p_2^* < 1$, $p_3^* > 1$, and the wave intensity at the fixed points given by $I_i^* = P - p_i^*$.

The stability of C_i^* is determined from the eigenvalues λ_i of the Jacobian matrix by linearizing the equations of motion (10a) and (10b) in the vicinity of each fixed point. Doing so, we find that the eigenvalues for C_1^* and $C_{2,3}^*$ are respectively

$$\lambda_1 = \pm \left(-\sqrt{2I_1^*} - \frac{1}{2I_1^*} \right)^{1/2}, \quad (13a)$$

$$\lambda_{2,3} = \pm \left(\sqrt{2I_{2,3}^*} - \frac{1}{2I_{2,3}^*} \right)^{1/2}. \quad (13b)$$

The eigenvalue λ_1 is imaginary for any value of I_1^* , which means that the fixed point $y_1^* = 0$ has elliptic stability. In addition, since $p_1^* < 0$, the physical condition $I_1^* = P - p_1^*$ implies that $I_1^* > P$ for any value of P .

When $I_2^* = I_3^* = 1/2$, the eigenvalues $\lambda_{2,3} = 0$, indicating a bifurcation point at $y_{2,3}^* = \pi$ that occurs for $P = 3/2$ and $p_2^* = p_3^* = 1$. For $I_2^* > 1/2$, the eigenvalue λ_2 is real, so that in $y_2^* = \pi$ the system has hyperbolic stability for any $P > 3/2$ with $0 < p_2^* < 1$. Finally, for $0 < I_3^* < 1/2$, the eigenvalue λ_3 is imaginary, indicating that at the same abscissa $y_3^* = \pi$ we also have elliptic stability for any $P > 3/2$ with $p_3^* > 1$.

The values of p_i^* at the fixed points (12) are obtained as a function of the total momentum P , i.e. $p_i^* = \pm 1/\sqrt{2(P-p_i^*)}$, so that we can describe the solutions at the equilibrium with the equation

$$(P - I_i^*)^2 I_i^* = 1/2. \quad (14)$$

As shown in Fig. 1, equation (14) selects the I_i^* values for which the cubic polynomial on the left-hand side assumes a given value. The blue line represents the stable solution at the elliptic fixed point at $y_1^* = 0$: this solution exists for any value of total momentum P . The black point at $P = 3/2$ shows a bifurcation, where two types of equilibrium coincide at the same fixed position $y_{2,3}^* = \pi$. After the bifurcation point, the red line corresponds to the unstable solution at the fixed position $y_2^* = \pi$, and the green line corresponds to the stable solution in the same fixed position $y_3^* = \pi$.

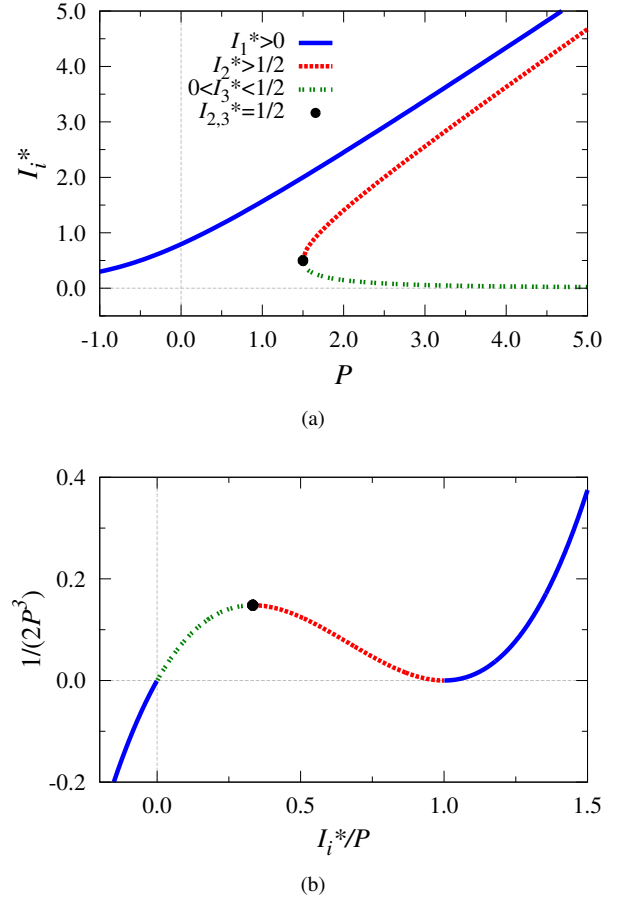


FIG. 1. (a) Bifurcation diagram of equation (14) for the $M = N = 1$ system. The blue (solid) line corresponds to the elliptic stable fixed point at $y_1^* = 0$. The black point at $I_{2,3}^* = 1/2$ and $P = 3/2$ corresponds to the bifurcation, and the red (dotted) and green (double-dotted) lines correspond, respectively, to the hyperbolic and the elliptic fixed points at $y_{2,3}^* = \pi$ after the bifurcation. (b) Roots of the normalized equation (14), $(1 - I_i^*/P)^2 I_i^*/P = 1/(2P^3)$.

The $M = N = 1$ system is integrable. Actually, solving (9) for $\cos y$ and squaring (8b) leads to the first order equation

$$\begin{aligned} \dot{p}^2 &= 2(P-p) \left[1 - \left(\frac{H - p^2/2}{\sqrt{2(P-p)}} \right)^2 \right] \\ &= 2P - H^2 - 2p + Hp^2 - \frac{p^4}{4}, \end{aligned} \quad (15)$$

which is solved analytically in terms of elliptic functions.³¹ Briefly, one finds a function \mathfrak{P} such that $p = \mathfrak{P}(t; p^*, P, H)$ by integrating (15), and a function \mathfrak{Q} such that $y = \mathfrak{Q}(t; p^*, P, H) = \text{Arcsin}[-\dot{p}/\sqrt{2(P-p)}] = \text{Arccos}[(p^2 - 2H)/\sqrt{8(P-p)}]$ modulo boundary conditions. One can also construct action-angle variables for each type of periodic trajectory.

The equilibrium points $p = p_i^* = \text{constant}$ for equation (15)

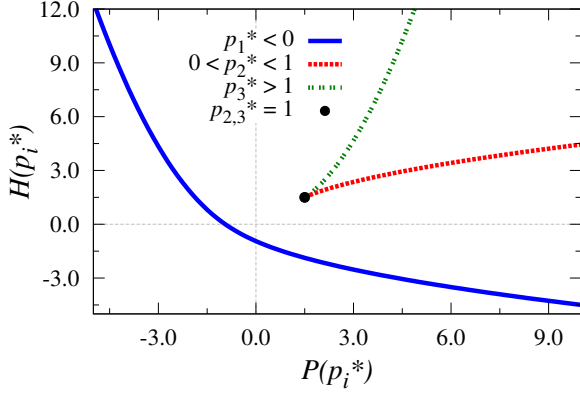


FIG. 2. Curves on plane (P, H) for equations (17).

are defined by the conditions

$$G(p_i^*) = 0, \quad \left. \frac{dG}{dp} \right|_{p=p_i^*} = 0, \quad (16)$$

with $G(p)$ the quartic polynomial on the right-hand side of (15). Solving (16) for the values of parameters H and P , we find parametrically given curves

$$P(p_i^*) = \frac{1 + 2p_i^{*3}}{2p_i^{*2}}, \quad H(p_i^*) = \frac{2 + p_i^{*3}}{2p_i^*}. \quad (17)$$

These curves on the (P, H) plane contain important information on the system dynamics.⁴³

The loci of equations (17) in plane (P, H) are shown in Fig. 2. As in Fig. 1(a), the blue (solid) curve represents the stable elliptic point at $y_1^* = 0$; the black point at $(P, H) = (3/2, 3/2)$ with $p_{2,3}^* = 1$ corresponds to bifurcation; the red (dotted) curve represents the parameters of the hyperbolic fixed point at $y_2^* = \pi$; and the green (double-dotted) line is associated with the elliptic fixed point also at $y_3^* = \pi$. After the bifurcation, for a given value of P , the energy of the stable (elliptic) fixed point at $y_1^* = 0$ is lower than the energy of the hyperbolic fixed point at $y_2^* = \pi$, and the latter, in turn, is lower than the energy of the elliptic fixed point at $y_3^* = \pi$. The topological changes described by the solutions of (14) in Fig. 1(a) and by (17) in Fig. 2 are presented in the phase portraits of the next section.

Moreover, for (P, H) on these curves, the evolution equation (15) reduces to

$$\dot{p} = \pm(p - p^*) \left(\frac{1}{p^*} - \frac{(p - p^*)^2}{4} \right)^{1/2}, \quad (18)$$

which can be solved in terms of elementary functions. Specifically, if $0 < p^* < 1$, this equation admits real-valued solutions for real time, describing motion on the separatrix of the hyperbolic fixed point. On the contrary, if $p^* < 0$ or if $p^* > 1$, equation (18) has no real-valued solution, as the associated fixed point is elliptic.

B. Phase portrait analysis for $N = M = 1$

The phase portrait of the system in the (p, y) variables is shown in Figure 3 and has special boundaries. Indeed, variable $y = x - \theta$ is 2π -periodic and the wave intensity must be positive so that $p \leq P$, and the portrait will be plotted over half a cylinder.

As already seen in the previous subsection, the fixed point at $y_1^* = 0$ has elliptic stability for all values of the total momentum P so that the dynamics of the system around the elliptic point is represented by closed trajectories.

The black line in the phase portraits represents the trajectory for which the wave intensity I passes through 0. The ordinate P for p does not correspond to a continuum of values for y , because equation (10a) is meaningless if $\cos y \neq 0$. Thus only abscissae $y = \pm\pi/2$ are permitted when $I = 0$, and then the wave phase is actually undefined. But the dynamics is well-defined in cartesian variables (X, Y) , and, if the wave turns out to vanish at a time, then $\dot{X}^2 + \dot{Y}^2 = 1$ implies that I cannot remain zero, i.e., the potential acting on the particle cannot remain flat. Actually, as the particle position is a smooth function of time, what occurs when I vanishes is that the wave phase jumps between $x - \pi/2$ and $x + \pi/2$, and the trajectory in (p, y) variables transits through this connection with $\dot{p} = 0$ and $\ddot{p} = -1$, so that the value $p = P$ is a non-degenerate local maximum of p along the trajectory. According to (9), this trajectory has energy $H = P^2/2$. The phase jump by π instantly interchanges the locations of the wave potential's trough and crest, which is a very efficient mechanism generating chaos and violent mixing in the system with more than one particle.³⁵

For $P < 3/2$, the black line separates the cylinder into two domains: the orbits rotating (clockwise) around the elliptic fixed point, and the orbits winding (toward the left) around the cylinder. For the value $P = 3/2$, the system has a saddle-center bifurcation at which an elliptic-hyperbolic pair coalesce, as shown by the black point in the bifurcation diagram, Figs. 1 and 2. The trajectory asymptotic to the bifurcation point is represented by the red line in Fig. 3(b).

For $P > 3/2$, we see two different types of stability at the same fixed point coordinate $y_{2,3}^* = \pi$. The upper fixed point is elliptic, circled by orbits rotating counterclockwise in the phase portrait. The lower fixed point is hyperbolic, and the lower branch of its separatrix winds (to the left) around the cylinder: from $t \rightarrow -\infty$, the particle leaves the crest of the wave potential, it passes at the bottom of the wave potential when the wave has its largest amplitude, and it asymptotes again the next crest of the potential for $t \rightarrow +\infty$, so that $\int_{-\infty}^{+\infty} \dot{y}(t) dt = -2\pi$. The upper branch of the separatrix is, for $3/2 < P < 3/4^{1/3}$, a counterclockwise loop around the elliptic fixed point, with $\cos(x - \theta)$ always negative: from $t \rightarrow -\infty$, the particle leaves the crest of the wave potential, it passes again at the same crest of the wave potential when the wave has its smallest amplitude, and it asymptotes again the same crest of the potential for $t \rightarrow +\infty$, so that $\int_{-\infty}^{+\infty} \dot{y}(t) dt = 0$.

Fig. 3(c) shows another special value of P for which the phase portrait changes: when $P = 3/4^{1/3}$, the points of null wave intensity belong to the separatrix of the X point ($y_2^* = \pi$,

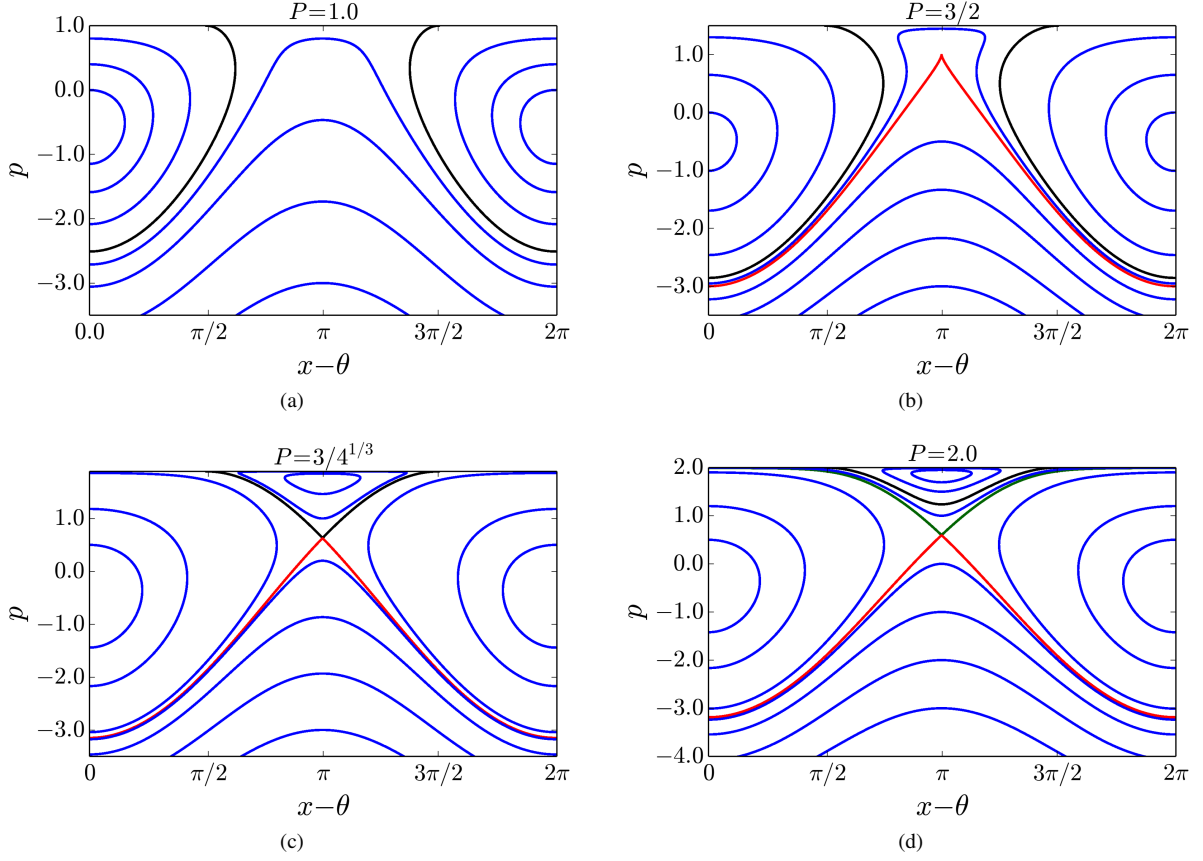


FIG. 3. Phase portrait with $N = 1$ for the single wave Hamiltonian (9). Panel (a) shows the case $P < 3/2$ (before the bifurcation), panel (b) shows the case $P = 3/2$ (at the saddle-center bifurcation), panel (c) corresponds to total momentum $P = 3/4^{1/3}$, for which the trajectory containing $I = 0$ coincides with the upper branch of the X point separatrix, and panel (d) shows the dynamics after the global bifurcation.

$p_2^* \sqrt{2(P - p_2^*)} = 1$). The trajectory for which this happens has energy $H_{I=0} = P^2/2$ (for passing through $I = 0$), and this energy must also be equal to the energy of the X point, i.e. $H_{I=0} = (p_2^*)^2/2 + \sqrt{2(P - p_2^*)}$ (where p_2^* is the X point momentum obtained by solving condition $p_2^* \sqrt{2(P - p_2^*)} = 1$). Thus, $P^2 = (p_2^*)^2 + 2\sqrt{2(P - p_2^*)} = (p_2^*)^2 + 2/p_2^*$, and the X point condition implies that $P = p_2^* + 1/(2(p_2^*)^2)$, so that $(p_2^*)^2 + 1/p_2^* + 1/(4(p_2^*)^4) = (p_2^*)^2 + 2/p_2^*$, i.e. $p_2^* = 4^{-1/3}$ and $P = 3/4^{1/3}$. Because this phase portrait connects two distinct points (the $I = 0$ point and the X point), the system undergoes a global bifurcation at this value $P = 3/4^{1/3}$.

For $P > 3/4^{1/3}$, the upper branch of the separatrix winds around the cylinder (to the right): from $t \rightarrow -\infty$, the particle leaves the crest of the wave potential, it passes at the bottom of the wave potential when the wave has its smallest amplitude, and it asymptotes the next crest of the potential for $t \rightarrow +\infty$, so that $\int_{-\infty}^{+\infty} \dot{y}(t) dt = 2\pi$. Moreover, for $P > 3/4^{1/3}$, the black line containing the points with $I = 0$ separates two domains: above it, trajectories circle counterclockwise around the elliptic fixed point in $y_3^* = \pi$, whereas trajectories wind around the cylinder (to the right) between it and the upper branch of the separatrix.

IV. THE SINGLE WAVE AND TWO PARTICLES

A. General aspects

The $M = 1, N = 2$ system is the first step towards the dynamics of the paradigmatic single wave model, where the case of many particles sheds much light on fundamental plasma instabilities, in particular the bump-on-tail. The reference Hamiltonian $H_{sc}^{2,1}$ (from now on, denoted simply H)

$$\begin{aligned}
 H &= \frac{p_1^2}{2} + \frac{p_2^2}{2} + \omega_0 \frac{X^2 + Y^2}{2} \\
 &\quad + \varepsilon Y(\sin x_1 + \sin x_2) - \varepsilon X(\cos x_1 + \cos x_2) \quad (19a) \\
 &= \frac{p_1^2}{2} + \frac{p_2^2}{2} + \omega_0 I - \varepsilon \sqrt{2I} (\cos(x_1 - \theta) \\
 &\quad + \cos(x_2 - \theta)) \quad (19b)
 \end{aligned}$$

describes the two particles interacting self-consistently with the wave. Again, a Galileo transformation enables us to set

$\omega_0 = 0$, leaving

$$H = \frac{p_1^2}{2} + \frac{p_2^2}{2} + \varepsilon(Y(\sin x_1 + \sin x_2) - X(\cos x_1 + \cos x_2)) \quad (20a)$$

$$= \frac{p_1^2}{2} + \frac{p_2^2}{2} - \varepsilon\sqrt{2I}(\cos(x_1 - \theta) + \cos(x_2 - \theta)). \quad (20b)$$

Finally, rescaling all variables as $t' = \lambda^{-1}t$, $x' = x$, $\theta' = \theta$, $p' = \lambda p$, $I' = \lambda I$, $P' = \lambda P$, $X' = \lambda^{1/2}X$, $Y' = \lambda^{1/2}Y$, $H' = \lambda^2 H$ shows that the coupling parameter can also be scaled away with $\varepsilon' = \lambda^{3/2}\varepsilon$. Thus we are left with three cases:

1. $\varepsilon = 0$: the system is uncoupled;
2. $\varepsilon = 1$: the coupling has unit strength and favors $x_{1,2} \sim \theta$ energetically;
3. $\varepsilon = -1$: the coupling has unit strength and favors $x_{1,2} \sim \pi + \theta$ energetically, but this can be absorbed in the change of variable $\theta' = \theta + \pi$.

The model is thus completely parametrized by total energy H and total momentum $P = p_1 + p_2 + (X^2 + Y^2)/2$ for $\varepsilon = 1$. From here on, we set $\varepsilon = 1$. A similar Hamiltonian was considered by del Castillo Negrete and Firpo^{35,42}, with a different wave-particle coupling. Our results complement theirs.

For the $M = N = 1$ model, the fact that the wave intensity must be positive implied that the particle momentum p was bounded from above by P . With two particles, total momentum P sets no bound on a single particle momentum since only $p_1 + p_2$ is bounded by P .

The original dynamics (19a) or (20a) has three degrees of freedom, with phase space $(\mathbb{T} \times \mathbb{R})^2 \times \mathbb{R}^2$, where particles evolve on the cylinder $\mathbb{T} \times \mathbb{R}$ and the harmonic oscillator (*viz.* the wave) evolves in the plane \mathbb{R}^2 . Given the two conserved quantities, the dynamics is restricted to 4-dimensional manifolds, and the motions generate Poincaré maps in 3-dimensional sections.

The equations of motion read

$$\dot{x}_r = p_r, \quad (21a)$$

$$\dot{p}_r = -X \sin x_r - Y \cos x_r = -\sqrt{2I} \sin(x_r - \theta), \quad (21b)$$

$$\dot{X} = \sin x_1 + \sin x_2, \quad (21c)$$

$$\dot{Y} = \cos x_1 + \cos x_2, \quad (21d)$$

$$\dot{\theta} = -(2I)^{-1/2}(\cos(x_1 - \theta) + \cos(x_2 - \theta)), \quad (21e)$$

$$\dot{I} = \sqrt{2I}(\sin(x_1 - \theta) + \sin(x_2 - \theta)). \quad (21f)$$

For $\omega_0 > 0$, the Hamiltonian (19b) is bounded from below: $|\cos(x_1 - \theta) + \cos(x_2 - \theta)| \leq 2$, so that

$$\begin{aligned} H &\geq \frac{p_1^2 + p_2^2}{2} - 2\sqrt{2I} + \omega_0 I \\ &= \frac{p_1^2 + p_2^2}{2} + \frac{\omega_0}{2}(\sqrt{2I} - \frac{2}{\omega_0})^2 - \frac{2}{\omega_0}. \end{aligned} \quad (22)$$

For $\omega_0 \leq 0$, the Hamiltonian (19b) is not bounded from below: one may have $x_1 = x_2 = \theta$, $p_1 = p_2 = 0$ and I arbitrarily large. Then $H = \omega_0 I - 2\sqrt{2I} \rightarrow -\infty$ as $I \rightarrow \infty$. However,

for fixed P , the Hamiltonian is bounded from below even for $\omega_0 \leq 0$:

$$\begin{aligned} H &\geq \frac{p_1^2 + p_2^2}{2} - 2\sqrt{2I} + \omega_0 I \\ &= \frac{(p_1 + p_2)^2 + (p_1 - p_2)^2}{4} - 2\sqrt{2}\sqrt{P - (p_1 + p_2)} \\ &\quad + \omega_0(P - (p_1 + p_2)) \\ &\geq \frac{(p_1 + p_2)^2}{4} - 2\sqrt{2}\sqrt{P - (p_1 + p_2)} \\ &\quad + \omega_0(P - (p_1 + p_2)), \end{aligned} \quad (23)$$

and the last two terms cannot diverge faster than the first one if P is bounded.

Given P and H , equation (23) implies that p_1 and p_2 are bounded, and equation (22) shows that I is bounded too. Since x_1, x_2 and θ vary on the unit circle, the constant (P, H) manifolds are compact.

This discussion about boundedness shows how important the conservation of momentum is. Moreover, it stresses how the notion of energy depends on the observer's viewpoint: a mere Galileo transformation changes the model from H bounded from below for any P (with $\omega_0 > 0$) to H bounded from below conditionally on a fixed P .

B. Poincaré section variables

The intersection of energy and momentum surfaces is compact for every (H, P) , for any fixed ω_0 . Indeed, the generalized coordinates (x_1, x_2, θ) range over a 3-torus. The generalized momenta must satisfy the above inequalities implying that neither p_1 nor p_2 can diverge, and hence $I = P - p_1 - p_2$ cannot diverge either.

For a fixed P , consider the reduced dynamics in terms of (y_1, y_2, p_1, p_2) , with $I = P - p_1 - p_2$ and $y_r = x_r - \theta$. Then

$$\dot{y}_r = p_r + \frac{\cos y_1 + \cos y_2}{\sqrt{2(P - p_1 - p_2)}}, \quad (24a)$$

$$\dot{p}_r = -\sqrt{2(P - p_1 - p_2)} \sin y_r, \quad (24b)$$

with the conserved Hamiltonian

$$H = \frac{p_1^2}{2} + \frac{p_2^2}{2} - \sqrt{2(P - p_1 - p_2)}(\cos y_1 + \cos y_2). \quad (25)$$

As the $N = 1$ case is recovered by setting $y_1 = y_2, p_1 = p_2$ and rescaling time, energy and coupling constant, let $\sigma = P/2$. With variables $z_1 = (y_1 + y_2)/2$, $z_2 = (y_1 - y_2)/2$, $w_1 = (p_1 + p_2)/2$, $w_2 = (p_1 - p_2)/2$, the Poisson brackets are

$$\begin{aligned} [f, g] &= \partial_{p_1} f \partial_{y_1} g - \partial_{y_1} f \partial_{p_1} g + \partial_{p_2} f \partial_{y_2} g - \partial_{y_2} f \partial_{p_2} g \\ &= \frac{1}{2}(\partial_{w_1} f \partial_{z_1} g - \partial_{z_1} f \partial_{w_1} g + \partial_{w_2} f \partial_{z_2} g + \\ &\quad - \partial_{z_2} f \partial_{w_2} g), \end{aligned} \quad (26)$$

so that Hamilton's canonical evolution equations read

$$\begin{aligned} \dot{g} = [H, g] &= (\partial_{w_1} \frac{H}{2}) \partial_{z_1} g - (\partial_{z_1} \frac{H}{2}) \partial_{w_1} g + \\ &\quad + (\partial_{w_2} \frac{H}{2}) \partial_{z_2} g - (\partial_{z_2} \frac{H}{2}) \partial_{w_2} g. \end{aligned} \quad (27)$$

Specifically,

$$\begin{aligned}\dot{z}_1 &= w_1 + \frac{\cos(z_1 + z_2) + \cos(z_1 - z_2)}{\sqrt{4(\sigma - w_1)}}, \\ &= w_1 + \frac{\cos z_1 \cos z_2}{\sqrt{\sigma - w_1}},\end{aligned}\quad (28a)$$

$$\dot{z}_2 = w_2, \quad (28b)$$

$$\begin{aligned}\dot{w}_1 &= -\sqrt{4(\sigma - w_1)} \frac{\sin(z_1 + z_2) + \sin(z_1 - z_2)}{2}, \\ &= -2\sqrt{\sigma - w_1} \sin z_1 \cos z_2,\end{aligned}\quad (28c)$$

$$\begin{aligned}\dot{w}_2 &= -\sqrt{4(\sigma - w_1)} \frac{\sin(z_1 + z_2) - \sin(z_1 - z_2)}{2}, \\ &= -2\sqrt{\sigma - w_1} \cos z_1 \sin z_2.\end{aligned}\quad (28d)$$

The new variables (w_1, w_2, z_1, z_2) are not canonically equivalent to the original ones (since the bracket undergoes a rescaling by $1/2$), but the quantity

$$\begin{aligned}E = H/2 &= \frac{w_1^2}{2} + \frac{w_2^2}{2} - \sqrt{\sigma - w_1} (\cos(z_1 + z_2) + \cos(z_1 - z_2)) \\ &= \frac{w_1^2}{2} + \frac{w_2^2}{2} - 2\sqrt{\sigma - w_1} \cos z_1 \cos z_2\end{aligned}\quad (29)$$

plays the role of a Hamiltonian in these new variables as the action differential of the system may be written as

$$\begin{aligned}dS &= \sum_r p_r dx_r + I d\theta - H dt \\ &= \sum_r p_r dy_r + P d\theta - H dt \\ &= 2 \left(\sum w_r dz_r + \sigma d\theta - E dt \right).\end{aligned}\quad (30)$$

Note that $E = H/2$ is also the energy per particle, like $\sigma = P/2$ is the momentum per particle.

The periodic boundary conditions $y_r \equiv y_r + 2\pi \bmod (2\pi)$ imply that the configuration space is a torus. The covering of this torus with cells of the form $z_r \equiv z_r + 2\pi \bmod (A_r)$ for an appropriate A_r is not consistent if one sets $A_1 = A_2 = \pi$ for both z_1 and z_2 . For the sake of safety, we set $A_1 = A_2 = 2\pi$, which implies that the new cells have a double area of that of the original ones, and two points in the cell (z_1, z_2) correspond to a single point in (y_1, y_2) .

We analyze the Poincaré sections at $z_2 \equiv 0 \bmod (2\pi)$. For a given σ , a point (w_1, z_1) in this section may correspond to different energies E , depending on w_2 . More precisely, when both particles have the same $(p, y) = (p_1, y_1) = (p_2, y_2)$, we have the $N = 1$ dynamics, with just a doubled mass and doubled coupling constant. This generates a family of solutions to the $N = 2$ case. But for $N = 2$ we have an arbitrary w_2 , and the energy $E = E_1 + w_2^2/2$ (with $E_1 = w_1^2/2 - 2\sqrt{\sigma - w_1} \cos z_1$ for $z_2 = 0$), so that the two-particle case always has more energy than the $N = 1$ case. Since E is conserved, the excess energy $w_2^2/2$ in the two-particle system may be taken as a perturbation parameter enabling chaos near the orbits of the integrable system.

The $z_2 = 0, w_2 = 0$ trajectory appears in the Poincaré section $z_2 = 0$ as the boundary of the domain accessible for a given total energy H . Its stability is governed by the linearized

equations

$$\dot{z}_1 = w_1 + \frac{\cos z_1}{\sqrt{\sigma - w_1}}, \quad (31a)$$

$$\dot{w}_1 = -2\sqrt{\sigma - w_1} \sin z_1, \quad (31b)$$

$$\delta \dot{z}_2 = \delta w_2, \quad (31c)$$

$$\delta \dot{w}_2 = -(2\sqrt{\sigma - w_1} \cos z_1) \delta z_2, \quad (31d)$$

where the (w_1, z_1) dynamics is master and the (w_2, z_2) dynamics is slave. Indeed, the Taylor expansion $\cos \delta z_2 = 1 - (\delta z_2)^2/2 + \dots$ implies that δz_2 cannot appear in the (w_1, z_1) dynamics.

This master-slave description is, for $(\delta w_2, \delta z_2)$, a linearized version of Boozer's analysis of the emergence of chaos in Hamiltonian systems.⁴⁴

If the (w_1, z_1) trajectory remains confined in the band $\cos z_1 > 0$ (or $-\pi/2 < z_1 < \pi/2$), then the small perturbation $(\delta z_2, \delta w_2)$ obeys a linear evolution equation with time-periodic coefficients of Hill's type, $\delta \ddot{z}_2 = -g(t)\delta z_2$ with a positive function $g(t)$. Though there may be resonances for some such (w_1, z_1) trajectories, the perturbation may remain bounded. Indeed, the Poincaré sections show nice KAM tori in this range (Fig. 4), and one checks that $E - E_1$ is positive definite for $\cos z_1 > 0$.

In contrast, when the (w_1, z_1) trajectory enters the band $\cos z_1 < 0$ (or $-\pi/2 < z_1 - \pi < \pi/2$), then the perturbation obeys $\delta \ddot{z}_2 = -g(t)\delta z_2$ with a negative function $g(t)$. During this time, the perturbation is amplified (and the more as z_1 approaches π), and the system may leave the linear regime. Then $\cos z_2$ is no longer close to 1, and the relative motion (w_2, z_2) feeds back upon the “master” variables. Such a process easily generates chaos, and one may expect that, soon enough, the trajectory approaches $z_1 \approx \pi$ and the associated hyperbolic point. As a result, one may expect a well-developed chaotic behavior for trajectories entering the band $\cos z_1 < 0$. Energetically, $E - E_1$ has an indefinite signature for $\cos z_1 < 0$.

The (w_1, z_1) trajectories which come close to $w_1 = \sigma$ are also likely to behave chaotically, because this line corresponds to $I = 0$, and on this line the angle z_1 spontaneously jumps by π to account for the sign reversal of both X and Y when the wave crosses null-amplitude. Then the corner of the wave cat's eye in original variables (x_r, p_r) suddenly becomes its center, and conversely, which is a very efficient mixing process.^{35,45}

C. Regular and chaotic trajectories

Figures 4 and 7 show the Poincaré section for different surfaces with constant energy. To simplify the analysis, we set the value of the total momentum P and we vary the value of the total energy H . The corresponding P and H values appear at the top of each figure.

Chaos in the self-consistent interaction of two particles ($N = 2$) with one wave ($M = 1$) is expected, since this is a non-integrable Hamiltonian system, and there is no nontrivial solution with a traveling wave.⁴⁶ Moreover, it is intuitive to think that typically chaos starts and is more intense in the

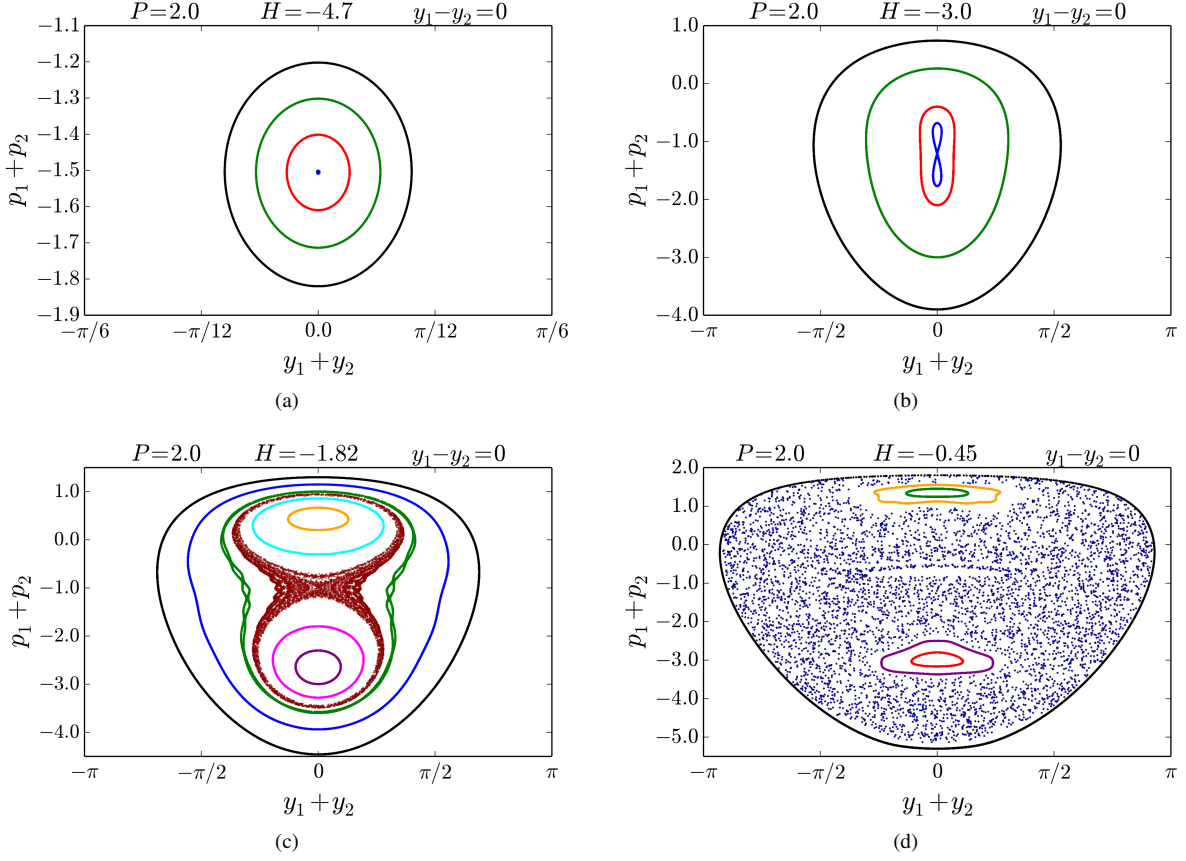


FIG. 4. Interception of trajectories with the Poincaré section located at $y_1 - y_2 = 0$ for negative H values. All panels in this figure represent the dynamics in the region of the elliptic fixed point at $y_1 - y_2 = 0$. The blue trajectory on the panel (a) is not a fixed point of the differential equations. It appears as a fixed point only in the Poincaré section defined at $y_1 - y_2 = 0$ for positive w_2 . Likewise, the hyperbolic point in the center of the blue trajectory similar to an “8” on panel (b) is not a fixed point of the differential equations, only of the Poincaré section. The total energy is increased from (a) $H = -4.7$ to (b) $H = -3.0$, (c) $H = -1.82$, (d) $H = -0.45$.

regions close to the separatrix of the $N = 1$ system.¹ In particular, the explicit solution for the separatrix can be used to prove nonintegrability of perturbations of this system using the Melnikov-Poincaré integral.^{47,48}

In our case, this would mean that the chaotic activity would be greater when the trajectory of the particles in the phase space passes close to the hyperbolic fixed point, located at $y_1 + y_2 = \pi$. Thus, if this scenario was the only relevant one, the intensity of chaos should gradually reduce as we approach the elliptic fixed point at $y_1 + y_2 = 0$.

However, as shown in Figure 4, the appearance of chaos does not follow this expectation, since we observe the emergence of chaos near the elliptic fixed point. Figure 4(a) shows the sections of the particles trajectories in the negative energy regime. The perturbation value, which is given by the difference in the initial velocities of the particles, increases from the black to the blue trajectory. In this scenario, the wave intensity is very large and the kinetic energy of the particles is low, which means that the particles oscillate in the bottom of the wave potential well.

For a very small difference between the initial condition of the velocities of the particles (perturbation), the two particles

“agglomerate” and move together so that the evolution can be understood as if there were only one particle ($N = 1$) in the system interacting with the wave. This dynamics is represented by the black trajectory in Fig. 4(a). The Fourier transform of the amplitude of the total momentum $p_1 + p_2$ of the particles for this trajectory, in Fig. 5(a), shows that the system then oscillates harmonically with a single frequency.

Now considering the dynamics of the blue trajectory (Figure 4(a)), which has the highest perturbation value for this energy surface, we find that, as we increase the disturbance in the system, the oscillation amplitude of the center of mass of the particles increases and the particles start oscillating in anti-phase with respect to each other. The relative motion of the particles with respect to the wave gives rise to a resonance, as shown by the Fourier transform in Figure 5(b). As seen in Figures 4(b) to 4(d), the contribution of this resonance is eventually enough to establish resonance overlap and chaos.

The emergence and intensification of chaotic activity when the trajectories of the particles are close to the elliptic fixed point, as shown in Figures 4(b) to 4(d), is not usually expected for the wave-particle system. About this unusual behavior, we can see on the transition from Figure 4(a) to 4(c) that, as

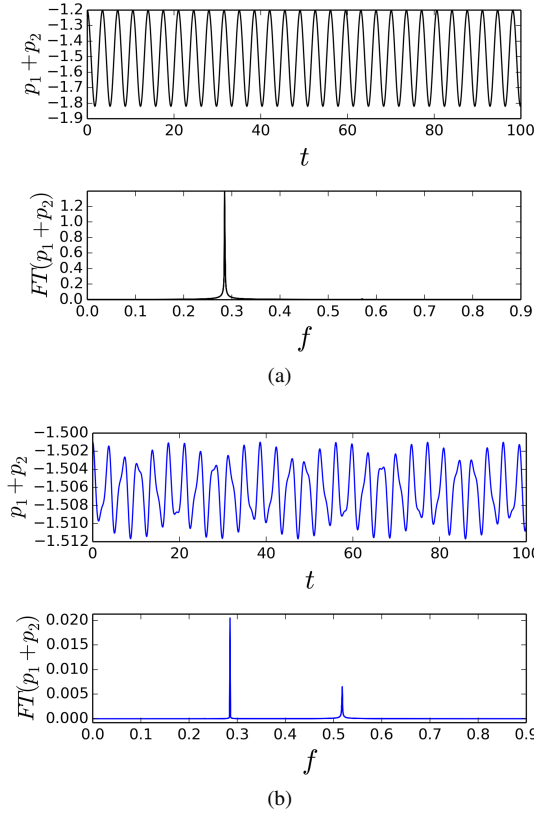


FIG. 5. Temporal evolution and Fourier transform of the particles total momentum for the (a) black and (b) blue trajectories in Figure 4(a).

the disturbance increases, some trajectories are deformed (see green trajectory in Fig. 4(c)), and others destroyed (see dark red chaotic trajectory in Fig. 4(c)). Although this phenomenon is unexpected near an elliptic fixed point, deformation and destruction of tori due to increased disturbance is predicted by the KAM theorem.⁴⁹ Furthermore, the Poincaré-Birkhoff theorem predicts that, when a resonant torus is destroyed (due to the increase in the perturbation), a sequence of periodic orbits will appear in the phase space, which alternate between elliptic (stable) and hyperbolic (unstable), generating periodic points in the Poincaré section. In this scenario, the hyperbolic points are related to the emergence of chaos, while the elliptic points become the center of stable regions, called islands of resonance, immersed in the chaotic sea.⁴⁹ When the perturbation is increased, the trajectories that contain an unstable point (similar to an "8" in Figure 4(b)) give rise to chaos in this region. In Figures 4(c) and 4(d), we can see islands surrounded by chaos.

Figures 6(a), 6(b) and 6(c) show the time evolution of the particles total momentum and its Fourier transform for the blue, dark red, and blue trajectories of the Figs. 4(b), 4(c) and 4(d), respectively. Despite the noise in the Fourier-transformed signal, the peak frequency and its harmonics still appear well defined. This may be related to the fact that, when one or both particles escape from the potential well of the wave (giving rise to a burst of chaos), they are easily re-

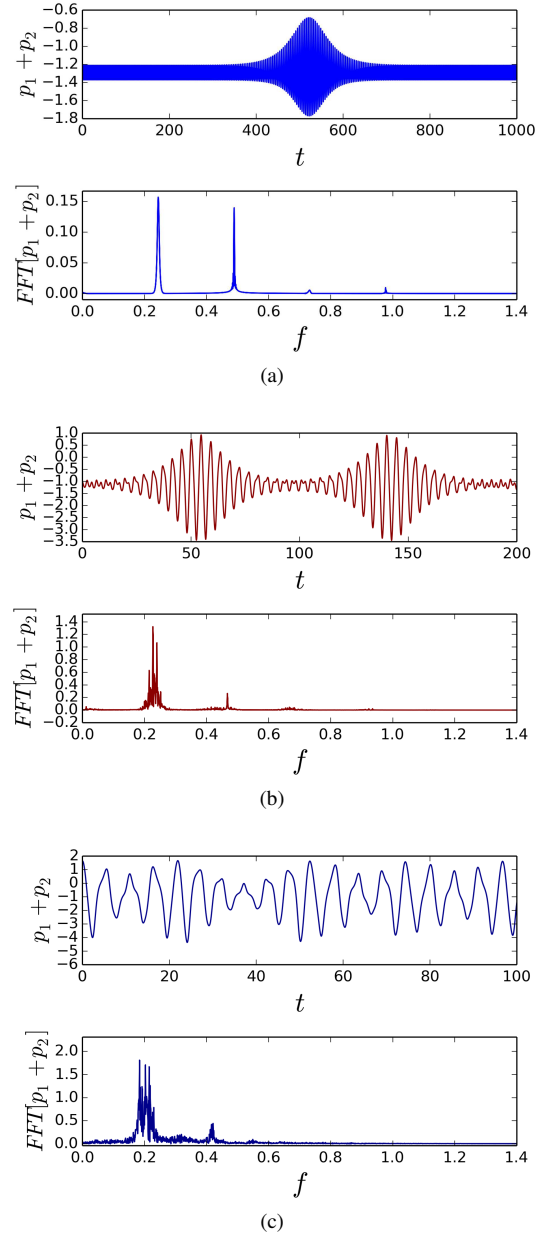


FIG. 6. Temporal evolution and Fourier transform of the particles total momentum for the (a) blue trajectory in Figure 4(b), (b) dark red trajectory in Figure 4(c), and (c) blue trajectory in Figure 4(d).

captured by the wave potential well. Hence, in this energy regime, the chaotic trajectory does not present a large excursion through phase space.

Poincaré sections for positive H values are shown in Figure 7. In this energy regime, the chaotic activity is already expected and is associated with separatrix chaos due to the hyperbolic fixed point at $y_1 + y_2 = \pi$. Indeed, close to the separatrix, the distances between resonances are very small, so that for small perturbation values the system can be driven quickly to the chaotic regime.^{37,48} In our case, in particular, this means that the dynamics becomes strongly chaotic even for small variations in the initial condition of the particles ve-

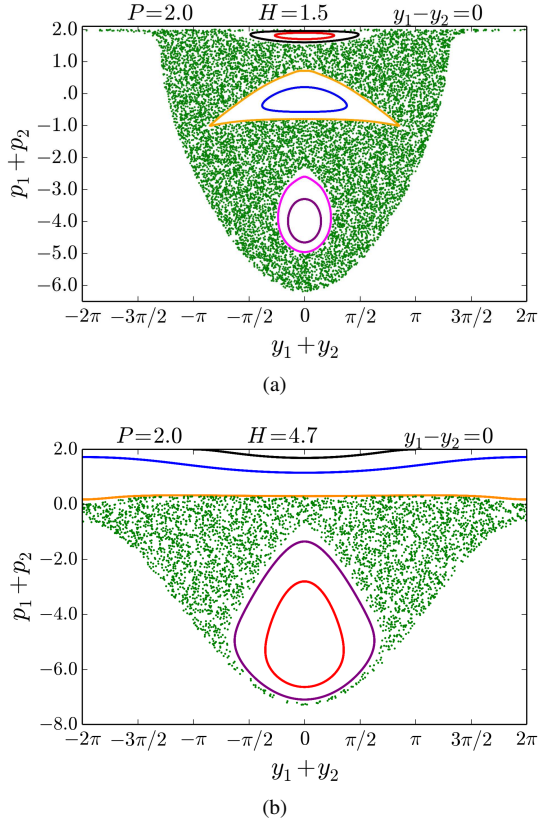


FIG. 7. Interception of trajectories with the Poincaré section located at $y_1 - y_2 = 0$ for positive H values. The total momentum value is $P = 2$ on both panels and the total energy increases from (a) $H = 1.5$ to (b) $H = 4.7$.

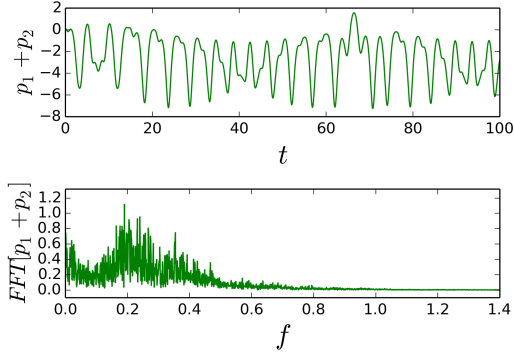


FIG. 8. Temporal evolution and Fourier transform of the particles total momentum for the green chaotic trajectory in Figure 7(b).

locities.

The temporal evolution of the particles total momentum and its Fourier transform for the green chaotic trajectory in Figure 7(b) is shown in Figure 8. Note that the signal in the Fourier transform looks just like a noise and it is not possible to point out a peak frequency. This may suggest that, in this chaotic regime, the particles are free to move in the phase space after gaining energy from the wave. The particles come back to exchange energy with the wave because the system is

conservative and motions occur on compact manifolds.

V. CONCLUSION

In this work, we analyze the regular and chaotic dynamics in the wave-particle interaction using the self-consistent Hamiltonian model.^{1,2} Considering the single wave model,^{27,28} we study the dynamics for $N = 1$ and $N = 2$ particles.

In the first stage, we analyze the self-consistent wave-particle interaction for $N = M = 1$. As this system is integrable, the phase space presents only regular trajectories. Integrable cases are important because they provide⁵⁰ a basic understanding of the coherent structures found for large N . As observed in subsection III B for different values of total momentum, the phase portrait topology of the $H = \text{constant}$ contours changes. For the specific value $P = 3/2$, the system has a bifurcation point at which an elliptic-hyperbolic pair of fixed points coalesce.

Bifurcation diagrams, Figs 1 and 2, provide a clear description of the system dynamics in terms of the equilibrium solutions. The analysis of the phase portrait complements the bifurcation diagrams. After the saddle-center bifurcation, a separatrix orbit appears and divides the phase portrait topology in three different domains, and the evolution of the system is different in each domain.

Moreover, we note that, as the trajectory in the phase portrait departs from the hyperbolic point, the system leaves the unstable linear regime; and, as the trajectory approaches the hyperbolic point from the trapped regime, it leaves the elliptic linear regime. For the special value $P = 3/4^{1/3}$, the system has a global bifurcation at which the energy line that contains $I = 0$ passes through the hyperbolic point.

For $N = 2$, we identify and analyze the emergence of chaos in a low-dimensional system. In this scenario, the discussion about the chaotic activity can be divided into two regions of the phase space, namely: close to the hyperbolic and elliptic fixed points. The appearance and intensification of chaos in the region close to the hyperbolic fixed point is usual, since for $N = 2$ the system is non-integrable, and the homoclinic tangle generated from a separatrix in a non-integrable Hamiltonian system is a skeleton near which chaotic transport develops. Chaos in this scenario is called separatrix chaos. In this region of phase space, the system is strongly conducive to the emergence of chaotic trajectories. In other words, the system presents strong sensitivity in the initial condition, so that the interaction quickly leads to chaos for small variation in the particles relative position and velocity (disturbance).

On the other hand, for wave-particle systems, the appearance of chaos near the elliptic fixed point is not typically expected. As noted in section IV, chaos in the vicinity of the elliptic fixed point arises in the negative energy regime. Since H is negative, the momentum p associated with the particles is low, whereas the wave intensity I is large since the total momentum P and total energy H are conserved quantities of the dynamics. This implies that, in the beginning, the particles should move in the stable well of the potential and, as we in-

crease the disturbance in the system, the particles would have more energy to exchange with the wave, but should remain trapped in the wave potential well.

The description of the wave-particle interaction in low-dimensional approximation proved to be fundamentally effective in the analyses of the basic characteristics of the system, especially those related to the emergence and intensification of chaos observed for $N = 2$. The analyses presented so far provide rich information on the dynamics of particles in the phase space due to their interaction with a single wave. So, this study becomes a basis for future analyses where the dynamics of many particles and many waves will be considered.

ACKNOWLEDGMENTS

The authors acknowledge discussions with Drs C. Chandre, X. Leoncini, L. H. Miranda F., T. M. Rocha Filho, and members of the *équipe turbulence plasma* in Marseille. They also thank anonymous reviewers for constructive comments. The Centre de Calcul Intensif d'Aix-Marseille is acknowledged for granting access to its high performance computing resources. JVG thanks Coordenação de Aperfeiçoamento de Pessoal de Nível Superior (CAPES) for financing her stay at Aix-Marseille Université (AMU) under the Programa de Doutorado Sanduíche no Exterior (PDSE), process No. 88887.307528/2018-00, and Conselho Nacional de Desenvolvimento Científico e Tecnológico (CNPq) for a doctoral fellowship at Universidade Federal do Paraná (UFPR), process No. 166914/2017-7. MCS thanks CAPES for financing her stay at AMU under the Programa Estágio Pós-Doutoral no Exterior, process No. 88887.307684/2018-00, and the Fundação de Amparo à Pesquisa do Estado de São Paulo (FAPESP) for a postdoctoral fellowship at Universidade de São Paulo (USP) under grant No. 2015/05186-0 (associated with grant No. 2018/03211-6). At the beginning of this work, YE enjoyed the hospitality of the grupo controle de oscilações at USP, and RLV and ILC enjoyed the hospitality of the *équipe turbulence plasma* at AMU, with the support from a COFECUB-CAPES grant Nos. 40273QA-Ph908/18 (COFECUB - Comité Français d'Évaluation de la Coopération Universitaire et Scientifique avec le Brésil), and 88881.143103/2017-01 (CAPES). RLV received financial support from CNPq, process No. 301019/2019-3. ILC acknowledges financial support from FAPESP under grant No. 2018/03211-6, and the CNPq under grant Nos. 407299/2018-1 and 302665/2017-0.

DATA AVAILABILITY

The data that support the findings of this study are available from the corresponding authors upon reasonable request.

¹Y. Elskens and D. Escande, *Microscopic dynamics of plasmas and chaos* (IoP Publishing, Bristol, 2003).

²D. F. Escande and Y. Elskens, "Microscopic dynamics of plasmas and chaos: the wave-particle interaction paradigm," *Plasma Phys. Control. Fusion* **45**, A115–124 (2003).

³D. G. Swanson, *Plasma kinetic theory* (CRC Press, Boca Raton, 2008).

⁴T. H. Stix, *Waves in plasmas* (Springer-Verlag, New York, 1992).

⁵C. F. F. Karney and A. Bers, "Stochastic ion heating by a perpendicularly propagating electrostatic wave," *Phys. Rev. Lett.* **39**, 550–554 (1977).

⁶G. R. Smith and N. Pereira, "Phase-locked particle motion in a large-amplitude plasma wave," *Phys. Fluids* **21**, 2253–2262 (1978).

⁷R. Balescu, *Transport processes in plasmas* (North-Holland, Amsterdam, 1988).

⁸S. Ichimaru, *Statistical Plasma Physics, Vol. I: Basic Principles* (CRC Press, Boca Raton, 2018).

⁹Y. Elskens, "Irreversible behaviours in Vlasov equation and many-body hamiltonian dynamics: Landau damping, chaos and granularity," in *Topics in Kinetic Theory (Toronto, 24.03-02.04.2004)*, edited by T. Passot, C. Sulem, and P. L. Sulem, Fields institute communications series 46 (Am. Math. Soc., Providence (RI), 2005) pp. 89–108.

¹⁰N. Besse, Y. Elskens, D. F. Escande, and P. Bertrand, "Validity of quasi-linear theory: refutations and new numerical confirmation," *Plasma Phys. Control. Fusion* **53**, 025012 (2011).

¹¹Y. Elskens, "Gaussian convergence for stochastic acceleration of particles in the dense spectrum limit," *J. Stat. Phys.* **148**, 591–605 (2012).

¹²A. V. Timofeev, "Cyclotron oscillations of plasma in an inhomogeneous magnetic field," *Sov. Phys. Uspekhi* **16**, 445 (1974).

¹³D. F. Escande, D. Bénisti, Y. Elskens, D. Zarzoso, and F. Doveil, "Basic microscopic plasma physics from N -body mechanics," *Rev. Mod. Plasma Phys.* **2**, 9 (2018).

¹⁴F. Doveil, D. F. Escande, and A. Macor, "Experimental observation of nonlinear synchronization due to a single wave," *Phys. Rev. Lett.* **94**, 085003 (2005).

¹⁵F. F. Chen, *Introduction to plasma physics and controlled fusion*, Vol. 1 (Plenum Press, New York, 1984).

¹⁶W. Herr, "Introduction to Landau damping," in *Advanced Accelerator Physics (Trondheim, 19-29.08.2013)*, arXiv:1601.05227, edited by W. Herr, CAS-CERN Accelerator School (CERN, Geneva, 2014).

¹⁷J. He, L. Wang, C. Tu, E. Marsch, and Q. Zong, "Evidence of Landau and cyclotron resonance between protons and kinetic waves in solar wind turbulence," *The Astrophysical Journal Letters* **800**, L31 (2015).

¹⁸C. H. K. Chen, K. G. Klein, and G. G. Howes, "Evidence for electron Landau damping in space plasma turbulence," *Nature communications* **10**, 1–8 (2019).

¹⁹L. D. Landau, "On the vibrations of the electronic plasma," *Yad. Fiz.* **10**, 25 (1946).

²⁰D. D. Ryutov, "Landau damping: half a century with the great discovery," *Plasma Phys. Control. Fusion* **41**(3A), A1–A12 (1999).

²¹P. Stubbe and A. I. Sukhorukov, "On the physics of Landau damping," *Phys. Plasmas* **6**, 2976–2988 (1999).

²²Y. Elskens, D. F. Escande, and F. Doveil, "Vlasov equation and N -body dynamics : How central is particle dynamics to our understanding of plasmas ?" *Eur. Phys. J. D* **68**, 1–7 (2014).

²³D. F. Escande, "Stochasticity in classical hamiltonian systems: universal aspects," *Phys. Rep.* **121**, 165–261 (1985).

²⁴M. C. de Sousa, F. M. Steffens, R. Pakter, and F. B. Rizzato, "Standard map in magnetized relativistic systems: Fixed points and regular acceleration," *Phys. Rev. E* **82**, 026402 (2010).

²⁵Y. H. Ichikawa, T. Kamimura, and C. F. F. Karney, "Stochastic motion of particles in tandem mirror devices," *Physica D: Nonlinear Phenomena* **6**, 233 – 240 (1983).

²⁶H. E. Mynick and A. N. Kaufman, "Soluble theory of nonlinear beam-plasma interaction," *Phys. Fluids* **21**, 653–663 (1978).

²⁷I. N. Onishchenko, A. R. Linetskii, N. G. Matsiborko, V. D. Shapiro, and V. I. Shevchenko, "Contribution to the nonlinear theory of excitation of a monochromatic plasma wave by an electron beam," *Soviet Phys. JETP* **11**, 281–285 (1971).

²⁸T. M. O'Neil, J. H. Winfrey, and J. H. Malmberg, "Nonlinear interaction of a small cold beam and a plasma," *Phys. Fluids* **14**, 1204–1212 (1971).

²⁹J. L. Tennyson, J. D. Meiss, and P. J. Morrison, "Self-consistent chaos in the beam-plasma instability," *Physica D* **71**, 1–17 (1994).

³⁰A. Antoniazzi, Y. Elskens, D. Fanelli, and S. Ruffo, "Statistical mechanics and Vlasov equation allow for a simplified hamiltonian description of single-pass free electron laser saturated dynamics," *Eur. Phys. J. B* **50**, 603–611 (2006).

- ³¹J. C. Adam, G. Laval, and I. Mendonça, “Time-dependent nonlinear Langmuir waves,” *Phys. Fluids* **24**, 260–267 (1981).
- ³²N. Carlevaro, G. Montani, and D. Terzani, “On the viability of the single-wave model for the beam plasma instability,” *EPL (Europhysics Letters)* **115**, 45004 (2016).
- ³³N. A. Yampolsky and N. J. Fisch, “Simplified model of nonlinear Landau damping,” *Phys. Plasmas* **16**, 072104 (2009).
- ³⁴Z. Huang and K.-J. Kim, “Review of X-ray free-electron laser theory,” *Phys. Rev. ST Accel. Beams* **10**, 034801 (2007).
- ³⁵D. del Castillo-Negrete and M.-C. Firpo, “Coherent structures and self-consistent transport in a mean field hamiltonian model,” *Chaos* **12**, 496–507 (2002).
- ³⁶D. Testa, A. Fasoli, D. Borba, M. de Baar, M. Bigi, J. Brzozowski, P. de Vries, JET-EFDA contributors, *et al.*, “Alfvén mode stability and wave-particle interaction in the JET tokamak: prospects for scenario development and control schemes in burning plasma experiments,” *Plasma Phys. Control. Fusion* **46**, S59–S79 (2004).
- ³⁷A. J. Lichtenberg and M. A. Lieberman, *Regular and stochastic motion* (Springer, New York, 1983).
- ³⁸E. Hairer, C. Lubich, and G. Wanner, *Geometric numerical integration: structure-preserving algorithms for ordinary differential equations* (Springer, Berlin, 2006).
- ³⁹G. M. Zaslavsky, *Hamiltonian chaos and fractional dynamics* (Oxford University Press, New York, 2005).
- ⁴⁰J. D. Crawford and A. Jayaraman, “First principles justification of a “single wave model” for electrostatic instabilities,” *Phys. Plasmas* **6**, 666–673 (1999).
- ⁴¹D. Farina, F. Casagrande, U. Colombo, and R. Pozzoli, “Hamiltonian analysis of the transition to the high-gain regime in a Compton free-electron-laser amplifier,” *Phys. Rev. E* **49**, 1603–1609 (1994).
- ⁴²D. del Castillo-Negrete, “Dynamics and self-consistent chaos in a mean field hamiltonian model,” in *Dynamics and Thermodynamics of Systems with Long-Range Interactions (les Houches, 18-22.02.2002)*, edited by T. Dauxois, S. Ruffo, E. Arimondo, and M. Wilkens (Springer, Berlin, 2002) pp. 407–436.
- ⁴³A. V. Bolsinov, A. V. Borisov, and I. S. Mamaev, “Topology and stability of integrable systems,” *Russian Mathematical Surveys* **65**, 259–318 (2010).
- ⁴⁴A. H. Boozer, “Arnold diffusion and adiabatic invariants,” *Phys. Lett. A* **185**, 423–427 (1994).
- ⁴⁵C. R. Menyuk, “Particle motion in the field of a modulated wave,” *Phys. Rev. A* **31**, 3282–3290 (1985).
- ⁴⁶Y. Elskens, “Finite- N dynamics admit no travelling-waves solutions for the hamiltonian XY model and single-wave collisionless plasma model,” in *ESAIM: Proceedings*, Vol. 10 (EDP Sciences, 2001) pp. 221–215.
- ⁴⁷V. Kozlov, “Integrability and non-integrability in hamiltonian mechanics,” *Russian Mathematical Surveys* **38**, 1–76 (1983).
- ⁴⁸J. Guckenheimer and P. Holmes, *Nonlinear oscillations, dynamical systems, and bifurcations of vector fields* (Springer, New York, 1983).
- ⁴⁹E. Ott, *Chaos in dynamical systems* (Cambridge university press, 2002).
- ⁵⁰R. Pakter and G. Corso, “Improving regular acceleration in the nonlinear interaction of particles and waves,” *Phys. Plasmas* **2**, 4312–4324 (1995).